


## 3D Attenuation Tomography of the Volcanic Island of Tenerife (Canary Islands)

J. Prudencio<sup>1,2</sup>  · J. M. Ibáñez<sup>2,3,4</sup> · E. Del Pezzo<sup>2,5</sup> · J. Martí<sup>6</sup> · A. García-Yeguas<sup>2,7,8</sup> · L. De Siena<sup>9</sup>

Received: 27 March 2015 / Accepted: 28 July 2015  
© Springer Science+Business Media Dordrecht 2015

**Abstract** This paper shows a new multidisciplinary interpretation approach to the internal structure of Tenerife Island. The central core of this work is the determination of the three-dimensional attenuation structure of the region using P-waves and the coda normalization method. This study has been performed using 45,303 seismograms recorded at 85 seismic stations from an active experiment (air gun shots) conducted in January 2007. The interpretation of these new results is done combining the new images with previous studies performed in the area such as seismic velocity tomography, magnetic structure, magnetotelluric surveys or gravimetric models. Our new 3D images indicate the presence of seismic attenuation contrasts, with areas of high and low seismic attenuation patterns. High seismic attenuation zones are observed both in shallow and in deeper areas. The shallowest area of Las Cañadas caldera complex (1–3 km thick) is dominated by high

---

✉ J. Prudencio  
janire@ugr.es

- <sup>1</sup> Earthquake Research Institute, University of Tokyo, 1-1 Yayoi, Bunkyo-ku, Tokyo 113-0032, Japan
- <sup>2</sup> Instituto Andaluz de Geofísica, University of Granada, Profesor Clavera 12, 18071 Granada, Spain
- <sup>3</sup> Dept. Física Teórica y del Cosmos, University of Granada, Fuentenueva S/N, 18001 Granada, Spain
- <sup>4</sup> Istituto Nazionale di Geofisica e Vulcanologia, Sezione di Catania -Osservatorio Etneo, 95125 Catania, Italy
- <sup>5</sup> Istituto Nazionale di Geofisica e Vulcanologia, Sezione di Napoli -Osservatorio Vesuviano, Via Diocleziano 328, 80124 Naples, Italy
- <sup>6</sup> Instituto de Ciencias de la Tierra Jaime Almera, CSIC, Lluís Solé Sabarís S/N, 08028 Barcelona, Spain
- <sup>7</sup> Dept. Física Aplicada, University of Cádiz, Av. Duque de Nájera 18, 11002 Cádiz, Spain
- <sup>8</sup> INVOLCAN, Antiguo Hotel Taoro, Parque Taoro 22, 38400 Puerto de la Cruz, Tenerife, Spain
- <sup>9</sup> School of Geosciences, Geology and Petroleum Geology, Meston Building, King's College, University of Aberdeen, AB24 3UE Aberdeen, Scotland

attenuation behavior, and it is interpreted as the combined effect of sedimentary and volcanoclastic deposits, multifracture systems and the presence of shallow aquifers. At the same time, the deeper analyzed area, more than 8 km below sea level, is dominated by a high attenuation pattern, and it is interpreted as the consequence of the effect of high-temperature rocks in the crustal–mantle boundary. This interpretation is compatible and confirmed by previous models that indicate the presence of underplating magma in this region. On the contrary, some low attenuation bodies and structures have been identified at different depths. A deep low attenuation central body is interpreted as the original central structure associated with the early stage of Tenerife Island. At shallower depths, some low attenuation bodies are compatible with old intermediate magmatic chambers postulated by petrological studies. Finally, in the north of the island (La Orotava valley) we can interpret the low attenuation structure as the headwall of this valley, supporting the idea that Las Cañadas caldera and this valley resulted from two different destructive processes.

**Keywords** Attenuation · Scattering · Tomography · Tenerife · Canary Islands

## 1 Introduction

Obtaining comprehensive models on the dynamics of volcanic systems, combining geological and geophysical data, is important to understand their past behavior and to predict their future activity. Different high-precision geophysical techniques, such as seismic tomography, magnetotelluric or gravimetry, provide good insights into the internal structure of volcanic systems and, when combined with stratigraphic, structural, petrological and geochemical data, may allow us to identify the main constraints on the dynamics of a particular volcano. Recently, seismological studies of volcanic regions are introducing a new and stable tool to add new and valuable information on the internal structure: seismic attenuation tomography. This technique is based on the study in heterogeneous media of the dissipation and scattering of the seismic waves (Del Pezzo 2008). The advantage of this procedure in comparison with the classical velocity tomography is that seismic wave attenuation is more sensible to the physical contrast of the medium (Sato et al. 2012). In the last few years, many examples highlight this evidence. Thus, Martínez-Arevalo et al. (2005) in their study of Etna volcano confirmed the presence of a high consolidate body in the central structure of the volcano that modifies the magma path in its ascent producing new adjacent vents. In a similar way, Del Pezzo et al. (2006) and De Siena et al. (2010) studied Vesuvius and Campi Flegrei volcanic regions, respectively, using attenuation properties. These authors confirmed the high contrast of attenuation associated with unconsolidated, highly fractured, hydrothermal systems and partial melt materials in both neighboring volcanic regions. In Mount St. Helens volcano, De Siena et al. (2013) used different attenuation techniques identifying important volcanic structures such as the main path of magma ascent from depth. In another sense, Prudencio et al. (2015) confirmed the effects of unconsolidated materials, hydrothermal system and partial melt rocks under Deception Island on the pattern of attenuation. In addition, in the same volcano, the contrast of the crystalline basement and volcanic structure observed by Zandomeneghi et al. (2009) is more clearly detected when separation of intrinsic and scattering attenuation is obtained (Prudencio et al. 2013b). These observations done in Deception volcano caldera are very close to others performed in a very similar volcano, but located in an

opposite region (Alaska against Antarctica), as those made in Okmok volcano (Ohlendorf et al. 2014). As De Siena et al. (2013) concluded: “these techniques represent the future of seismic volcano imaging.”

Tenerife Island is the largest, highest and the most complex island of Canary archipelago (Spain). In terms of its historical eruptions records, at least seven eruptions have been reported (Romero-Ruiz 1991) in the last 500 years. The Holocene eruptive record includes several tens of monogenetic eruptions and at least 16 eruptions from the central complex Teide–Pico Viejo (Carracedo et al. 2007; García et al. 2014). The scientific importance of this island is evidenced by the large number of geological, geophysical and geochemical studies performed on it in recent decades. Despite the large number of studies, there is a non-unique model of the evolution of the island and neither of its internal structure, and even the origin of the whole archipelago is still a close topic and few theories could be considered at present as potentially valid (e.g., Fullea et al. 2015).

In the present work, we perform a seismic attenuation tomography of Tenerife Island using P-waves and the coda normalization method (De Siena et al. 2014). Data used in this study were obtained by an active seismic experiment performed in 2007 (Ibáñez et al. 2008) and were used to obtain a high-resolution velocity tomography of the same region (García-Yeguas et al. 2012). The objective of this paper is to provide new information on the inner structure of the island that could permit us to better understand the volcanic framework of the region. This information will be interpreted jointly with other geological and geophysical evidence and will allow us to propose an advanced model of the internal structure of the island. Since the results of seismic attenuation are robust and reliable, we are certain that this new interpretation will help significantly in the improvement of the knowledge of the region.

## 2 Geological and Geophysical Framework

### 2.1 Geological Introduction

Tenerife is the largest (2058 km<sup>2</sup>) and highest (3718 m) island of the Canarian archipelago (Fig. 1). The geological evolution of Tenerife involves the construction of two main volcanic complexes: a basaltic shield complex (>12 Ma to present, Abdel-Monen et al. 1972; Ancochea et al. 1990; Thirlwall et al. 2000) and a central complex (<4 Ma to present, Fúster et al. 1968; Araña 1971; Ancochea et al. 1990; Martí et al. 1994). The basaltic shield complex is mostly submerged and forms about 90 % of the volume of the island, continuing at present its subaerial construction through two rift zones (Santiago Rift Zone and Dorsal Rift Zone, Fig. 1). The central complex comprises the Cañadas edifice (<4–0.18 Ma), a composite volcano characterized by several explosive eruptions of highly evolved phonolitic magmas, and the active Teide–Pico Viejo twin stratovolcanoes (0.18 ka to present) (Fig. 1). These last have evolved from basaltic to phonolitic and have mostly undergone effusive and explosive activity. The Cañadas caldera, in which the Teide–Pico Viejo stratovolcanoes stand, truncated the Cañadas edifice and was transformed by several vertical collapses, which were occasionally associated with lateral collapses of the volcano flanks (Martí et al. 1994, 1997; Martí and Gudmundsson 2000).

Recent volcanic activity is mostly represented by monogenetic basaltic volcanism located along the rift zones or scattered throughout the southern part of the island

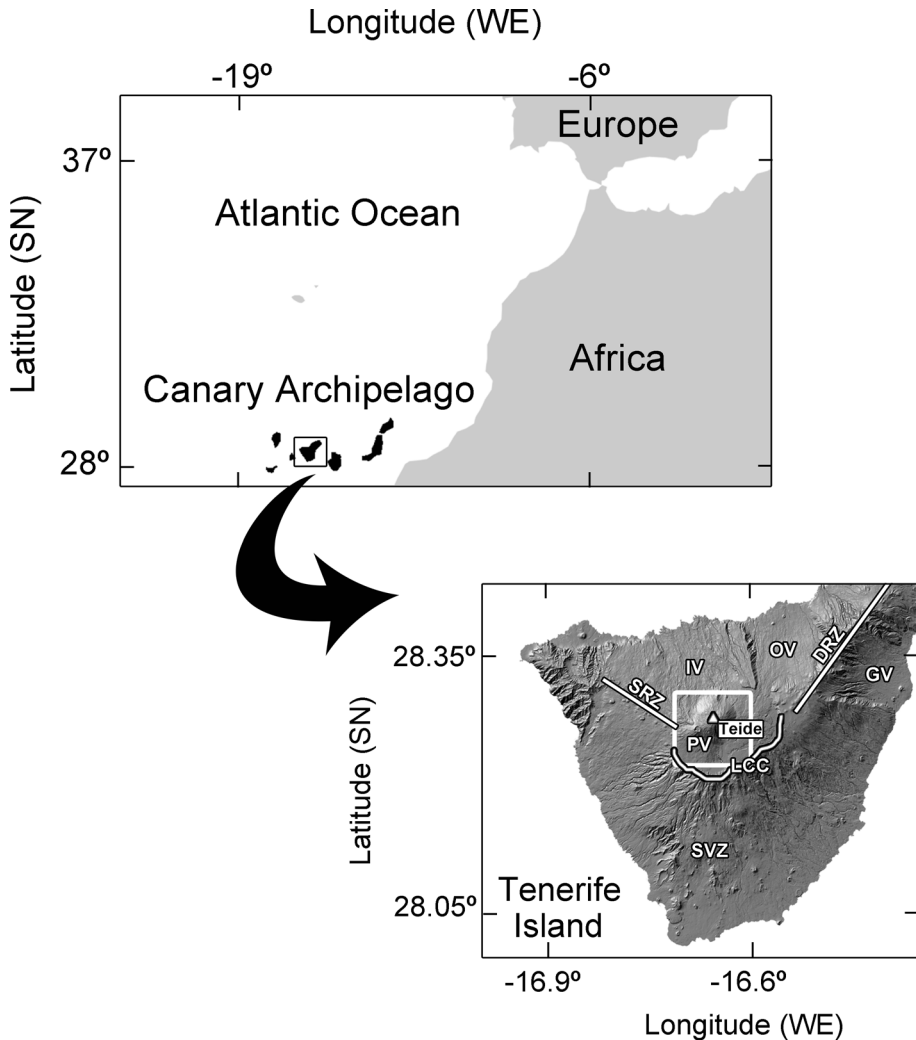


**Fig. 1** Regional setting and location of Tenerife Island in the Canary Islands archipelago (Spain). *White triangle* corresponds to the position of Teide volcano, *white lines* correspond to rift position, and Las Cañadas wall is also marked with *white line*. IV Icod Valley, OV Orotava Valley, SRZ Santiago Rift Zone, DRZ Dorsal Rift Zone, PV Pico Viejo, LCC Las Cañadas Complex, GV Guimar Valley, FASF Fasnía-Arafo-Siete Fuentes eruption and SVZ Southern Volcanic Zone [modified from Fig. 1 of Martí et al. (2012)]. We marked the higher-resolution area of Fig. 10

(Southern Volcanic Zone, Fig. 1) and, by the Teide–Pico Viejo stratovolcanoes (Fig. 1), with basaltic to phonolitic emissions (Martí et al. 2008).

The evolution of subaerial volcanism on Tenerife has been controlled mainly by the ENE–WSW and NW–SE oriented tectonic trends (Martí et al. 1996). Evidence comes from geophysical studies of the oceanic basement around and below the Canary Islands (Dash and Bosshard 1969; Bosshard and MacFarlane 1970; Verhoef et al. 1991; Mezcueta et al. 1992; Roest et al. 1992; Watts et al. 1997; Mantovani et al. 2007) and from dikes

distribution and the alignments of recent mafic vents. The predominance of these tectonic trends on Tenerife during its whole history suggests the importance of a long-lived regional tectonic control on the ascent of mantle-derived magmas and the distribution of volcanism.

Morphologically, the island of Tenerife is characterized by the superposition of the two volcanic complexes, basaltic shield and Las Cañadas edifice, which confer the characteristic pyramidal profile to the island. However, it is also important to mention the existence of four large depressions formed during destructive episodes and that correspond to the Las Cañadas caldera at the central part of the island and to the landslides valleys of Guimar, to the south, and La Orotava and Icod to the north (Fig. 1).

As indicated above, Tenerife has been the focus of several volcanological, geological, geochemical and geophysical studies in recent years. In the bibliography, there are recent works that provide a complete and well-structured review of them, such as Soler-Javaloyes and Carracedo (2013), Piña-Varas et al. (2014) or García et al. (2014).

In the present review, we will focus our description on those works that will help us to better understand and interpret our results, which basically are works on magnetic properties, magnetotellurics and seismic tomography.

## 2.2 Magnetic Properties

Recently, Blanco-Montenegro et al. (2011) presented a 3D structural model of Tenerife Island based on high-resolution aeromagnetic data. These authors identify a central basaltic shield that they interpreted as the origin of the island. This structure supports the model of a unique origin of the island in opposition to the three-armed rift system that could be present in the early stage of the island. Additionally, they identified the existence of consolidated dikes surrounding this central shield, interpreted as the consequence of magma intrusion from the early volcanic phases of the island. Additionally, in the shallower part of the island they identify some geometries that can be interpreted as round local landslides. Finally, they support the idea that the origin of the Las Cañadas caldera is associated with a vertical caldera collapse.

## 2.3 Magnetotelluric Properties

Pous et al. (2002) in their magnetotelluric study of Las Cañadas caldera found an area with high conductive anomaly that was interpreted by the existence of highly fractured rocks and fossil hydrothermal alteration located parallel and close to the caldera wall marking the position of the structural border of the caldera. Additionally, they identified two main shallow aquifer zones in this area. These results support the theory of multiple vertical collapse origin of the area. Similar results were observed by Coppo et al. (2008) using a more complete audio-magnetotelluric sounding profiles. They confirmed that Las Cañadas caldera structure is the result of at least three vertical collapses of different volcanic edifices which occurred during the last million years. Piña-Varas et al. (2014) studied the resistivity structure of Tenerife using different magnetotelluric surveys. They observed several areas with low resistivity values that mainly are associated with the presence of many geothermal systems. They performed a preliminary correlation with P-wave velocity models that also is the topic of the unpublished paper (García-Yeguas et al. 2015, in preparation). These authors found a deep area of medium resistivity values that are interpreted as potential partial melt region that could be the energy source of the hydrothermal activity.

## 2.4 Seismic Tomography and Seismic Studies

García-Yeguas et al. (2012) presented the first seismic tomography image of Tenerife Island using active seismic data obtained in the TOM-TEIDEVS experiment (Fig. 2) carried out in January 2007 (Ibáñez et al. 2008). The inversion of these data permits us to obtain a 3D velocity model from the top of the island (Teide–Pico Viejo–Cañadas complex) to 8–10 km below sea level. One of the main conclusions of this work is the presence of an unique high-velocity structure at the maximum resolve depths in the center of the island. This central structure characterized by high P-wave velocity was interpreted in concordance with other observations and the hypothesis made, for example, by Martí et al. (1994), Ablay and Kearey (2000), Pous et al. (2002), Gottsmann et al. (2008) or Geyer and Martí (2010) that postulate the presence of a single basaltic shield and, therefore, the formation of Tenerife arising from a single central volcanic structure. This interpretation is in agreement with Blanco-Montenegro et al. (2011). The surrounding and shallower regions are characterized by low-velocity structures which are associated with unconsolidated materials, hydrothermal alterations and the residual effects of recent volcanic

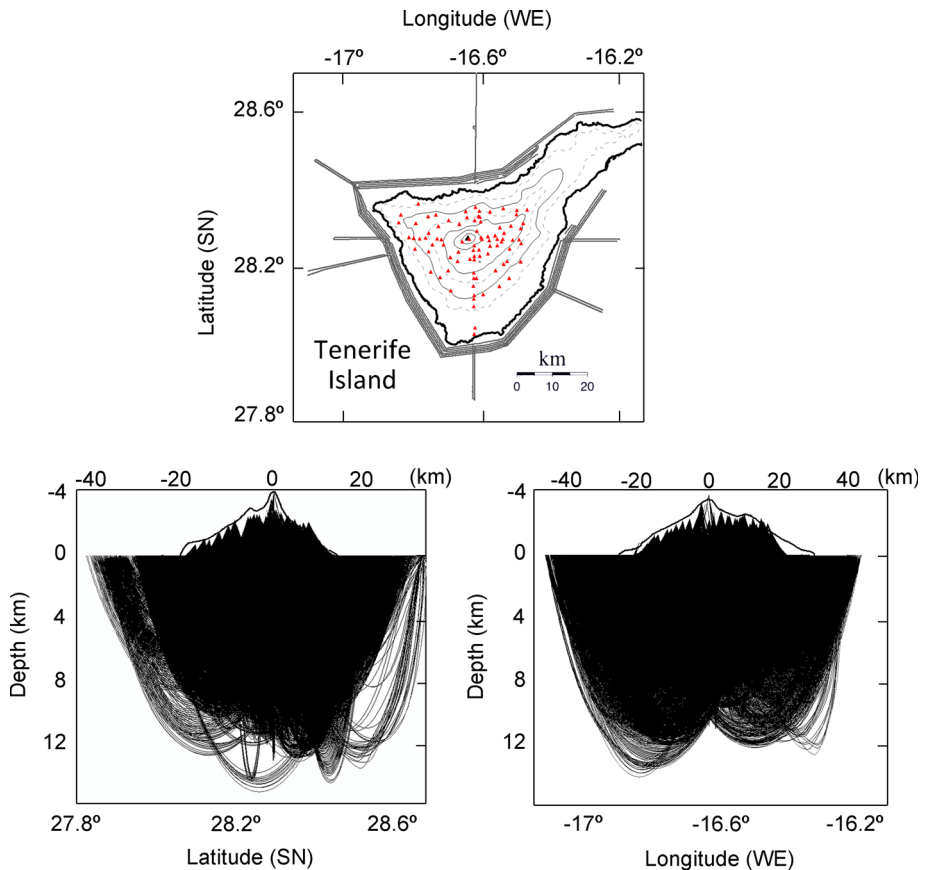


**Fig. 2** Configuration of TOM-TEIDEVS seismic tomography experiment. Stations are represented with *red triangles*, and shot locations with *gray dots*. 3D source station ray paths obtained by using Thurber-modified ray-bending approach are represented

eruptions. Prudencio et al. (2013a) obtained 2D regional distribution of seismic attenuation separating scattering and intrinsic contribution ( $Q_i^{-1}$  and  $Q_s^{-1}$ , respectively). As their main results, we can mention the existence of a region in the middle of Tenerife Island with low attenuation interpreted as the effect of intermediate/deep consolidate rocks. Surrounding this central body, there are several areas dominated by high attenuation effects. These external areas, also characterized by low P-wave velocity, were interpreted as complex fractured regions, hydrothermal alteration and the presence of volcanoclastic deposits, among others. In the whole island, scattering phenomena are more important (in terms of attenuation contribution) than intrinsic attenuation. De Barros et al. (2012) analyzed the potential effects on secondary arrivals produced by possible structures that generate scattered waves. They used the same dataset of García-Yeguas et al. (2012), and they identified two main bodies: one located at 7–9 km b.s.l. in the north part of the island and other at 1–4 km b.s.l. below the Cañadas caldera. They associate this shallow structure with a potential phonolitic storage area that could feed the Teide–Pico Viejo complex in the past. The presence of important structures that produce coherent scattered waves in Tenerife was already observed, also at shallow regions, by Del Pezzo et al. (1997). At deeper zones, Lodge et al. (2012) studied received functions recorded with the same seismic stations as used by the above authors. They found magmatic underplating beneath Tenerife Island and areas of low velocity that are interpreted as partial melt regions at depth 8–10 km b.s.l. These observations are in agreement with a previous study of Dañoibeitia and Canales (2000). These authors found two regions of low velocity below the main volcanic edifice: the shallower one, located around 4–8 km b.s.l., and the deeper one, characterized by low crustal P-wave velocity and located near the crustal-mantle boundary. They located this area between 17 and 25 km b.s.l., and it is interpreted as a magma underplating below Tenerife Island. The natural seismicity of the island at present is very low (Almendros et al. 2000, 2007) and also due to the reduced number of permanent seismic stations in the island, seismic source models are not too accurate. Recently, Domínguez Cerdeña et al. (2011) relocated the seismic activity associated with a strong seismic swarm which occurred during 2004–2005. These authors proposed a source model of this seismic swarm in which a possible magma intrusion at depth around 4 km (b.s.l.) takes place in the central part of the island below Teide volcano. The seismicity is the brittle response of the medium due to the effect of the increase in the pressure due to magma and gases movement. This magma intrusion was observed neither with the magnetic inversion nor with the seismic velocity tomography.

### 3 Data and Method

#### 3.1 Data

In this study, we used initially the dataset used to obtain 3D velocity structure by García-Yeguas et al. (2012) consisting of 103,750 waveforms. In Fig. 3, we show four recordings produced by shots located in the north and registered at stations 14, 75, 40 and 51 of TOM-TEIDEVS experiment. These stations are located either on or around Teide volcano. The corresponding waveforms show good signal-to-noise ratio after filtering data in the 4- to 8-Hz frequency band (central frequency 6 Hz).

The selection of the unique frequency band used (4–8 Hz) has been performed on the basis of previous consideration done on the same dataset by García-Yeguas et al. (2012)

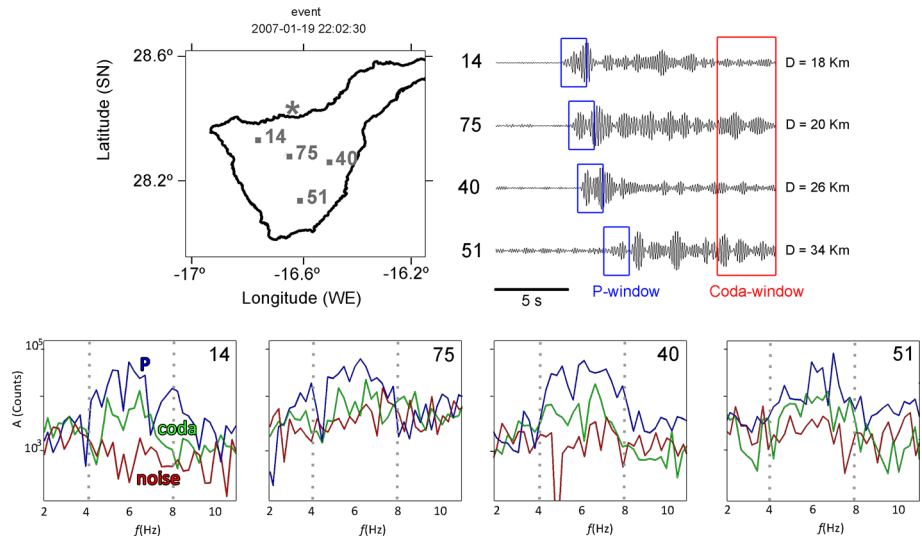


**Fig. 3** Four examples of vertical records of a seismic shot produced on the January 19, 2007, located in the north of Tenerife (*gray star*) and recorded at four onland seismic stations 14, 75, 40 and 51 (*gray boxes*). P window and coda window lengths used in the analysis are represented with *blue* and *red squares*, respectively. The *panels on the bottom* show the P-wave (*blue line*), coda (*green line*) and noise (*red line*) spectra for each seismogram. We marked the frequency band analyzed in the present work by *dashed line*

who found that the signal-to-noise ratio is largely acceptable in this band around the P-wave first arrival. We checked that the signal-to-noise ratio is sufficient in the whole seismogram utilized for the present analysis in this band and decided to restrict the analysis to this frequency band on the basis of the following considerations: (1) At frequencies lower than 4 Hz, coherent surface wave trains may introduce some bias in the estimation of the coda parameters; (2) at frequencies higher than 8 Hz, the anthropogenic noise may alter the coda envelope at long lapse time, thus introducing further bias. The selection of a unique (restricted) lapse time range (up to 20 s) is due to the necessity of investigating the smallest possible earth volume containing the Tenerife volcanic complex. Longer lapse times, on the other hand, would have reduced the number of available seismograms, due to the decrease in the signal-to-noise ratio at lapse times higher than 20 s.

### 3.2 Velocity Model and Ray Tracing

García-Yeguas et al. (2012) used the waveform dataset produced by the TOM-TEIDEVS active seismic experiment (Ibáñez et al. 2008) to invert 3D distribution of absolute P-wave velocities under the island. P-wave travel times are inverted using the code ATOM-3D, a tomography algorithm adapted by Koulakov (2009) for the 3D tomographic inversion based on active seismic data. The velocity model is distributed on a set of nodes whose distance depends on ray density and spans an area of  $40 \times 40 \text{ km}^2$ . The minimum node spacing is set at 0.7 km, and a continuous velocity distribution, necessary for the application of the ray tracing, is obtained by linear interpolation.

On this velocity model, we used a Thurber-modified ray-bending approach developed by Block (1991) which is an extension of Um and Thurber (1987). This approach has been recently applied by De Siena et al. (2010) in Campi Flegrei. The vertical ray distribution is



plotted in Fig. 2. This ray tracing algorithm has recently been tested and applied to active waveform data by Prudencio et al. (2015) at Deception Island. Between the surface and a depth of 12 km, a count of ray density confirms the applicability of attenuation tomography between depths of  $-2.2$  and 12 km. Therefore, the velocity and attenuation models are comparable if we use a grid having the same lateral extension of the first grid described by García-Yeguas et al. (2012).

### 3.3 P-wave Attenuation Tomography with the Coda Normalization Method

We use the coda normalization (CN) method to measure the single-path attenuation coefficient or, equivalently, the S-wave quality factor,  $Q_s$ . The earliest version of this method (Aki 1980) was utilized to calculate the space average S-wave attenuation in Japan. It is based on the concept of “coda normalization,” that in turn is based on the phenomenological coda wave properties. Aki (1980) showed that normalizing the direct S-wave spectrum for that of coda waves around a given “lapse time” (the time spanned from the origin time along the coda), the source intensity, the site transfer functions and the instrument transfer functions disappear in the ratio. More recently, Yoshimoto et al. (1993) showed that the direct P-wave spectrum can be normalized in the same way and extended the CN method to the measurement of P-wave attenuation coefficient. It is also noteworthy that the CN method can be successfully applied to separate frequency bands of the seismic spectrum, providing Q-estimates as a function of frequency (Aki 1980; Yoshimoto et al. 1993). The details of the application of CN method to single-path attenuation estimates are reported first in Del Pezzo et al. (2006) and successively in De Siena et al. (2009) and De Siena et al. (2010). Here, a brief review of the method is reported.

The energy spectrum around the frequency  $f_c$  of the P- or S-direct wave train,  $E^{P,S}(f, r)$ , for the  $k$ th ray connecting source  $i$  with receiver  $j$  at distance  $r$  can be written as:

$$E_{ij}^{P,S}(f_c, r) = S_i(f_c)\theta_{ij}(\vartheta, \phi)I_j(f)T_j(f)G_{ij}(f)\exp\left(-2\pi f_c \int_k \frac{dl}{v(l)Q^{P,S}(l)}\right) \quad (1)$$

where  $S_i$  is the source spectrum,  $\theta_{ij}(\vartheta, \phi)$  is the radiation pattern term,  $I_j$  is the instrument transfer function,  $T_j$  is the site transfer function,  $G_{ij}$  is the geometrical spreading term,  $v$  is the velocity, and  $Q^{P,S}$  is the quality factor. The line integral is extended to the  $k$ th ray.

The correspondent coda wave spectrum, around the lapse time,  $t_c$ , is given by (Aki 1980):

$$E^c(f_c, t_c) = S_i(f)I_j(f)T_j(f)P(f, t_c) \quad (2)$$

where  $P(f_c, t_c)$  is a function describing the scattering process. It can assume any analytical form, depending on the scattering model assumed (Del Pezzo et al. 2006). Applying logarithms to the ratio of Eqs. 1 and 2 and grouping some terms, we obtained the following relationship:

$$\frac{1}{\pi f_c} \ln\left(\frac{E_k^{P,S}(f_c, r)}{E^c(f_c, t_c)}\right) = K(f_c, t_c, \theta, \phi) - \frac{2}{\pi f_c} \gamma \ln(r_k) - 2 \int_k \frac{dl}{v(l)Q(l)} \quad (3)$$

where we have assumed a geometrical spreading coefficient,  $\gamma$ , which we invert together with the attenuation parameters (La Rocca et al. 2001; Morozov 2011; De Siena et al. 2014). The term  $K$  of Eq. 3 describes the effect of the source radiation pattern and depends

**Fig. 4** Input (*top left*) and output of the checkerboard test are shown on five *horizontal slices* taken at different depths (2.2 km a.s.l and 0.6, 3.4, 6.2 and 9 km b.s.l.). Tenerife Island contour is over-imposed on each *panel*. In the 2.2 km a.s.l. *panel (top right)*, the position of the *vertical sections* of next figures are shown

on the scattering model assumed. The effect of the source radiation pattern can be ignored if the signal analysis window is chosen wide enough that a proportion of the focal sphere is effectively sampled, as indicated by Del Pezzo et al. (2006). Additionally, in our data analysis we will use shots generated by air guns mounted in an oceanographic vessel, so that the source dimension can be assumed as point-like, and the radiation pattern as uniform. Therefore, the effects of radiation pattern are neglected.

For the present inversion, we will use a highly realistic velocity model to trace rays derived from the velocity seismic tomography of the region using the same dataset. Along a ray path, it is well known that the geometrical spreading coefficient,  $\gamma$ , may change, due to the perturbation of the wave front in the complex medium. We instead used the average geometrical spreading coefficient that we assumed to be that associated with a spherical wave front. Therefore, the changes in geometrical spreading may be incorporated into the changes in scattering  $Q$  (velocity fluctuations). Despite the trade-off between  $Q$  scattering and gamma (an effect that is widely observed in the literature), both parameters are associated with the same velocity fluctuations. A wider discussion about this theme can be found in De Siena et al. (2010).

There is an additional number of effects we assume into the estimation of  $Q$ . Focusing–defocusing (Nolet 2008) interference and other may all included into  $Q$  scattering. Therefore, inferred  $Q$  anomalies take implicitly into account the multiplicity of such effects. Similar observations were carried out by several authors such as Ibáñez et al. (1993), Akinci et al. (1995a) and Akinci et al. (1995b). These authors point out that the geometrical spreading and quality factor  $Q$  are strongly coupled, in the sense that the estimate of  $Q$  depends on  $\gamma$  and vice versa. Direct measurements of the geometrical spreading factor show that  $\gamma$  depends on the density of heterogeneities (Ibáñez et al. 1993), possibly affecting the scattering  $Q$  estimate rather than the intrinsic  $Q$  (e.g., Akinci et al. 1995a).

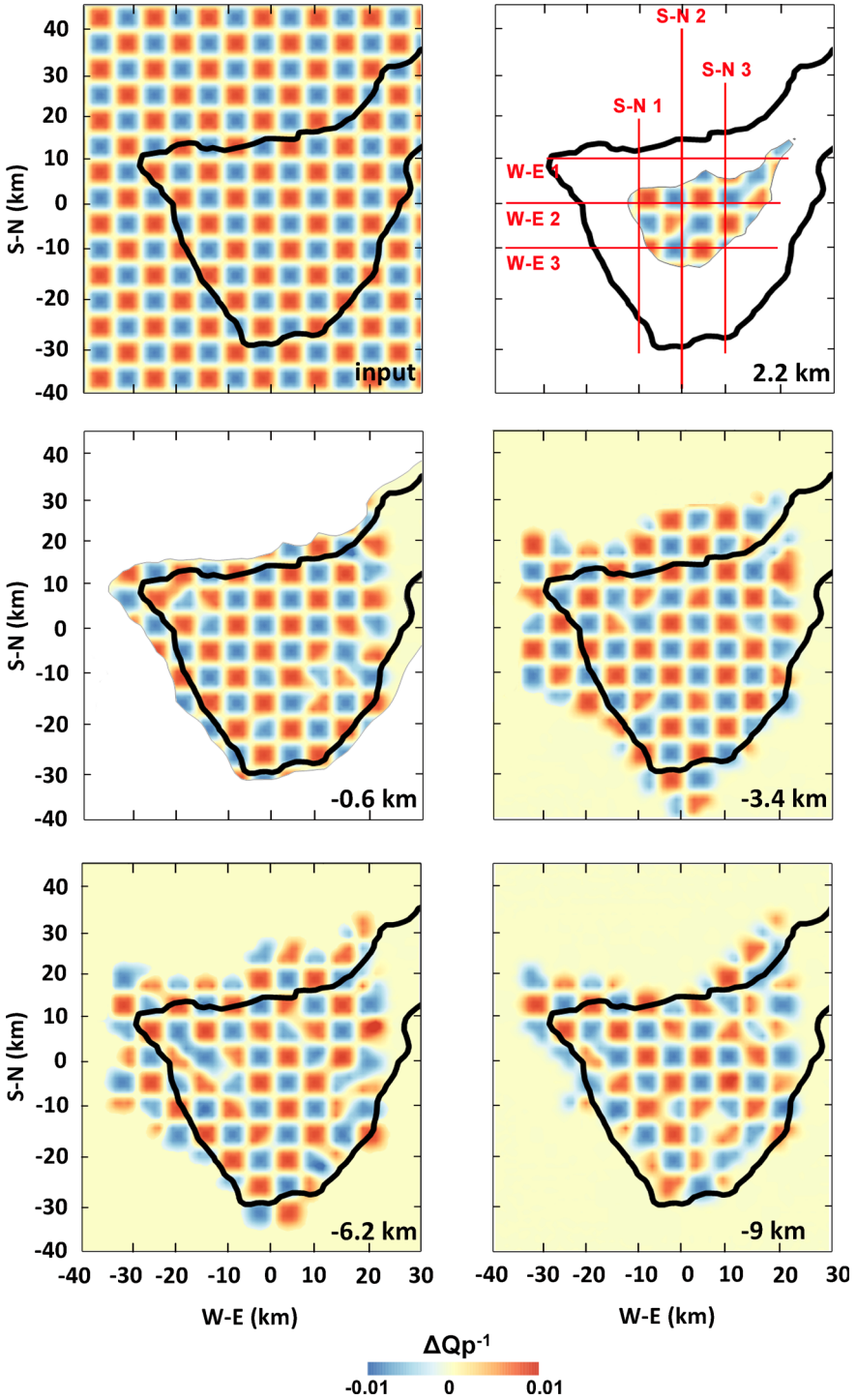
We invert the P-to-coda energy ratios with the MURAT code in a single-step inversion (De Siena et al. 2014). We set the start time of the coda time window duration (3 s) to a lapse time of 17 s. The P-energy time window is set to 1.5 s. The inversion of the energy ratios for the average parameters provides an average  $Q_p$  of 125. According to the resolution tests performed in the next section, the optimum size of the grid inversion is the use of cells of dimension of  $2.8 \times 2.8 \times 2.8$  km. In the following, we represent the variations with respect to the inverse of the average quality factor in the 3D space ( $\Delta Q_p^{-1}$ , in %).

## 4 Resolution, Stability and Robustness Tests

In order to check both robustness of the algorithm and the reliability, stability and resolution of the results, we perform (1) a checkerboard test, (2) a jackknifing test, (3) a test of the influence of the velocity model on results and (4) a synthetic anomaly test mimicking the results.

### 4.1 Checkerboard Test

In order to test the resolution of the entire region, we performed the well-known checkerboard test, whose results are shown in Fig. 4 (horizontal slices) and Fig. 5 (vertical



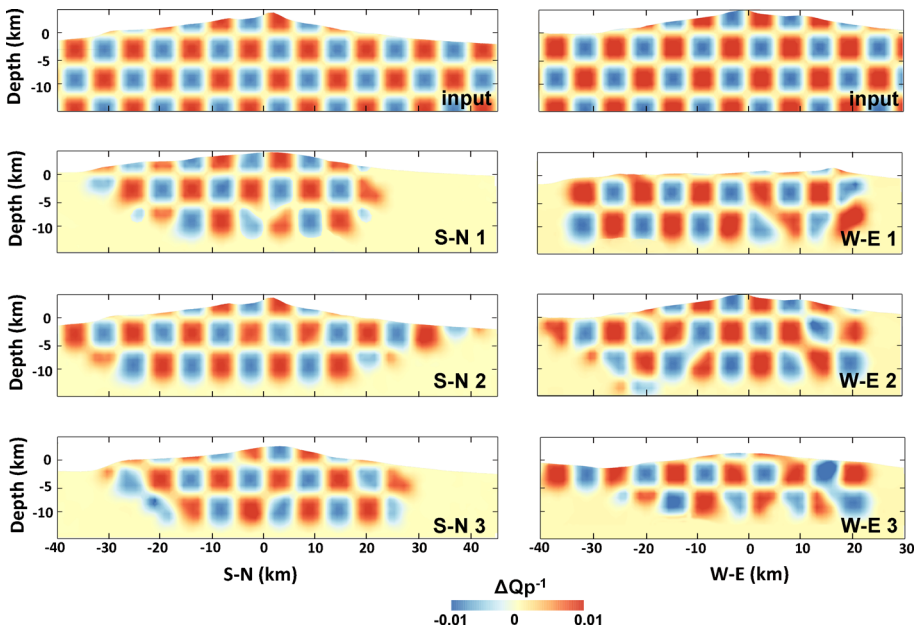


**Fig. 5** Input and output of the checkerboard test are shown for six *vertical* sections: three in S–N direction and three in W–E direction (see Fig. 4). The *vertical* scale is enlarged for clarity

sections). We generated synthetic *P*-to-coda energy ratios, and we added Gaussian random error with zero mean and 3 times the standard deviation. We inverted the synthetic data using blocks crossed by at least 10 rays with 2.8 km node spacing, starting at 2.2 km, and having quality factors equals to 100 or 1000. The checkerboard test results are well resolved in all obtained depths. In the horizontal slices, some external regions 6.2 km b.s.l. have a limited resolution that will not affect our final interpretation.

## 4.2 Jackknifing Test

To test the robustness of the data, we applied a jackknifing test consisting in the random removal of different percentages of data. The results of the test are shown in Fig. 6a–c. As can be observed, the main attenuation patterns do not change up to a 40 % removal of the data. The large number of events used gives us a strong stability of our final images that will be unaffected by potential lack of data.

## 4.3 Influence of Velocity Model

In order to check the influence of the velocity model on our attenuation results, we proceeded to randomly disturb it using some amount of noise. The procedure was to introduce some percentage of random variation in the 3D velocity model and to check the potential variations of the 3D attenuation model. The non-perturbed model is shown in Fig. 6d. We introduced a 5 and 10 % of random variation (uncorrelated Gaussian noise) to the original velocity model, and the obtained attenuation images (Fig. 6e, f) are almost identical to the original. This result demonstrates that our attenuation model is not coupled

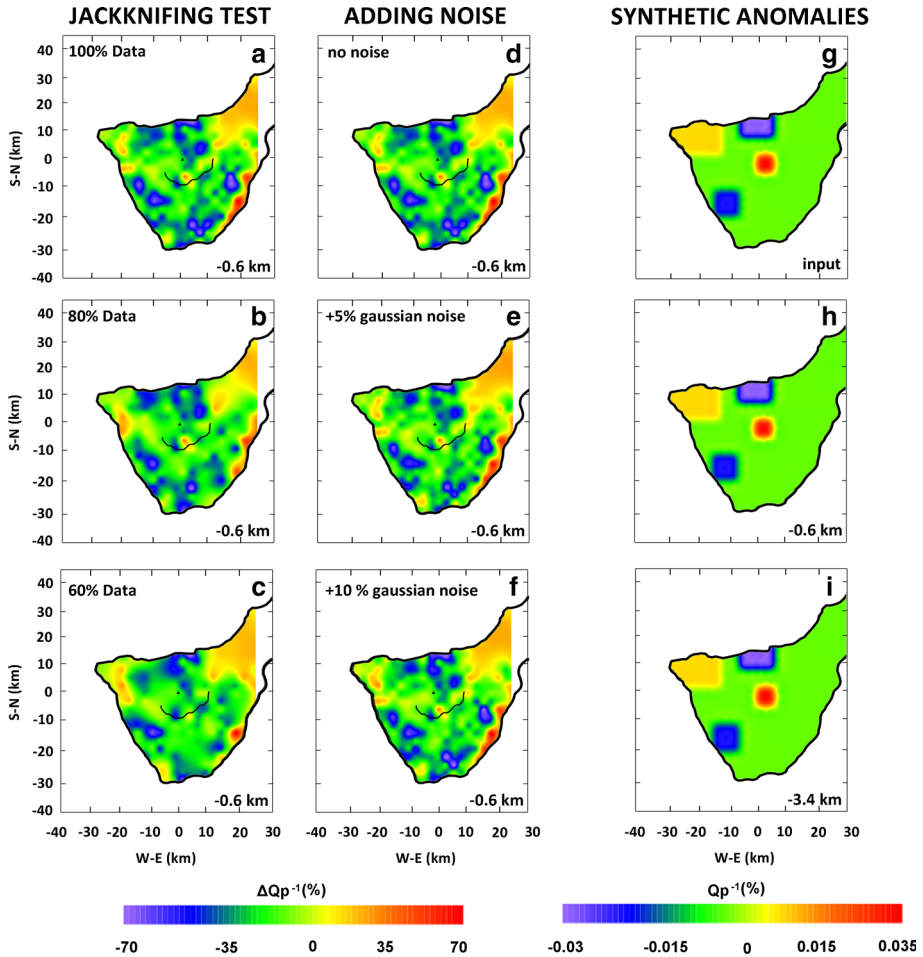


**Fig. 6** Different stability and robustness tests are shown: jackknifing test images with 100 % of the data (a), 80 % of the data (b) and 60 % of the data (c); velocity model influence test with no noise added (d), with +5 % of Gaussian noise (e) and with +10 % of Gaussian noise (f); and synthetic anomaly test input (g) and two horizontal slices through the output of the test at 0.6 and 3.4 km b.s.l. (h, i)

(no trade-off) with the velocity model, and the observed stability could be again associated with the large number of used data.

#### 4.4 Synthetic Anomaly Test

We also tested the resolution of our results by assuming different synthetic anomalies of high and low attenuation and different size. We imposed  $10 \times 20 \times 6 \text{ km}^3$  very low attenuation anomaly in the north coast,  $10 \times 10 \times 5 \text{ km}^3$  low attenuation anomaly in the southwestern region,  $20 \times 15 \times 8 \text{ km}^3$  high attenuation anomaly in the northwestern zone and  $5 \times 5 \times 5 \text{ km}^3$  very high attenuation anomaly in the central part of Tenerife Island. We add the same amount of Gaussian random error to the synthetic  $P$ -to-coda energy ratios calculated from the checkerboard test and inverted the synthetic data. The obtained results

are shown in Fig. 6g–i. All the anomalies are well reproduced which points out the good resolution of the region under study. The high density of rays provides us a good tool to solve with quality and confident the area under study.

## 5 Results and Discussion

The association of seismic attenuation anomalies to the corresponding rock properties is at present a complex task. Nowadays, the geological interpretation of the tomographic images is mostly based on physical interpolations and qualitative considerations, even if laboratory experiments and measurements are providing new evidences among their relationship. Vanorio et al. (2005) report a detailed discussion about the rock physics parameters and their relationship with seismic velocities at Campi Flegrei caldera (Southern Italy), giving insights into the dependence of  $V_p$  and  $V_s$  velocity from pore fluid pressure, porosity and temperature. More difficult is the interpretation of the attenuation anomalies. Total  $Q$  (the parameter which is generally represented in attenuation tomography as the present study) is the combination of intrinsic  $Q$  and scattering  $Q$ . The separate estimate of these two parameters is needed for a correct discrimination between temperature effects (lowering intrinsic  $Q$ , see De Lorenzo et al. 2001) and the contribution of strong heterogeneities (lowering scattering  $Q$ , see Sato et al. 2012). Moreover, the S-wave and P-wave attenuate in a different way in the same rock typology.  $V_p$  is relatively unaffected by the presence of fluid elements in the rock matrix, while a strong decrease in  $V_s$  velocity should be presented. Intrinsic  $Q$  for P-waves should hardly change, while a strong decrease in both P- and S-waves' scattering  $Q$  should be presented. We report some examples of possible interpretations in Table 1, which can be useful when multiple images based on different seismic attribute measurements are jointly available in the same region.

### 5.1 Tenerife Island $Q$ values

The inversion of the energy ratios for the average parameters provides an average  $Q_p$  of 125. In general, this average  $Q$  value is low in comparison with the expected average  $Q$  value for the Earth's crust (Sato et al. 2012). According to the resolution test performed in Sect. 4, the optimum size of the grid inversion is the use of cells of dimension of  $2.8 \times 2.8 \times 2.8$  km. In Fig. 7, we plot the five horizontal slices obtained from 2.2 km (above sea level) to the maximum depth of 9 km (below sea level). In Figs. 8 and 9, we show six vertical sections: 3 in S–N direction and 3 in the W–E direction as indicated in Fig. 4b.

**Table 1** Different values of P- and S-wave velocity and attenuation parameters and  $V_p/V_s$  ratio and its possible interpretation based on scientific papers reporting such interpretations

$V_p$	$V_s$	$Q_p^{-1}$	$Q_s^{-1}$	$V_p/V_s$	Interpretation
L	L	H	H	L	Fractured porous zone, typically on surface (e.g., Gudmundsson et al. 2004)
H	?	H	?	?	Fractured zone with the presence of fluids (e.g., De Gori et al. 2005)
L	L	H	H	A/H	Magma, fluids (e.g., Schurr et al. 2003)
L	L	H	L	L/A	Presence of gasses (e.g., Hansen et al. 2004)
H	H	L	L	A	Compact zone, typically at high depth (e.g., Eberhart-Phillips et al. 2005)
H	?	L	?	?	Volcanic conduit (e.g., De Gori et al. 2005)

Observing Fig. 8, the inner attenuation structure of Tenerife Island has several areas of high and low seismic attenuation contrast (red and blue areas, respectively). In the present discussion, we will describe in detail those we consider the most relevant, or due to their high contrast in the attenuation values, or because we can associate them with other geophysical, petrological or geological evidences of their existence and nature. These anomalies will be marked as H and L (high and low seismic attenuation) in the following figures. The rest of the non-described anomalies will be integrated in a further multidisciplinary study (García-Yeguas et al. 2015 in preparation) where these authors will integrate new geophysical and geological evidences that could help to interpret them. We can highlight the following main characteristics:

1. At shallower depths (over 5–6 km b.s.l.), Tenerife Island is mainly characterized by a low seismic attenuation structure (the general green color observed in Figs. 8 and 9). This observation is mostly common in several volcanic areas studied such as Mt. Vesuvius (De Siena et al. 2009; Tramelli et al. 2009), Campi Flegrei (De Siena et al. 2010) or Etna volcano (Martínez-Arevalo et al. 2005; Alparone et al. 2012). In general, this low attenuation, that also is coincident with the high-velocity structure, is interpreted as the response of consolidate and cold materials, as expected of classical stratovolcanoes.
2. At larger depths (underneath 6 km b.s.l.), high seismic attenuation dominates in the hole region (orange and red color in the bottom of Fig. 8). The observed low  $Q$  values can be associated with the potential presence of warmer materials with plastic behavior. Previous studies (e.g., Watts et al. 1997; Dañobeitia and Canales 2000; Lodge et al. 2012) have identified the possible existence of magma underplating beneath Tenerife Island analyzing seismic and other geophysical evidences. These authors identified the Moho below Tenerife at a depth around 15–18 km locating the magma underplating around or upon the Moho. In these studies, several discontinuities are observed such as crust-sediment or sediment-volcanic edifice. These zones are optimal for magma accumulation. This evidence is also confirmed with petrological analysis of mafic rocks which show differentiation characteristics (Ablay 1997; Neumann et al. 1999; Thrilwall et al. 2000).
3. At very shallow depths (close to the surface), we can identify a few areas with high seismic attenuation (e.g., H1 anomaly of Figs. 7 and 8). This anomaly is located just in the Las Cañadas caldera edifice. According to geophysical studies of Coppo et al. (2008), Coppo et al. (2010), Piña-Varas et al. (2014) and Villasante-Marcos et al. (2014), the caldera is filled by unconsolidated rocks and highly fractured material from Teide–Pico Viejo stratovolcanoes. Additionally, they identified in the caldera the presence of hydrothermally altered rocks and shallow aquifers. It is remarkable that H1 anomaly has a very similar geometry of these complex and altered structure. However, the resolution used in Fig. 8 cannot allow us to observe additional details. It is also worth mentioning that the contrast in seismic attenuation values surrounding the H1 anomaly could be identified as the limit of the caldera depression. Similar observations of the effect of shallow unconsolidated material have been done in Deception Island (Prudencio et al. 2015), Okmok volcano (Ohlendorf et al. 2014) or Campi Flegrei (De Siena et al. 2010).
4. A remarkable result is the identification in the inner part of Tenerife Island of several structures characterized by very low attenuation, L1, L2 and L3 of Figs. 7, 8 and 9. These low attenuation structures are usually identified as consolidate cold magmatic bodies, e.g., Etna (Martínez-Arevalo et al. 2005), Vesuvius (Tramelli et al. 2009).

**Fig. 7** Results of the attenuation tomography are shown for the five *horizontal slices* taken at different depths: **a** +2.2 km, **b** −0.6 km, **c** −3.4 km, **d** −6.2 km and **e** −9 km. The *color scale* show the variations (in percentage) of the attenuation model with respect to the average quality factor. The high and low attenuation anomalies discussed in the text are shown as *white squares* and *white labels* (H1, H2, L1, L2, L3, L4). In **e panel** (−9 km b.s.l.), the position of the *vertical sections* of the next figure are shown

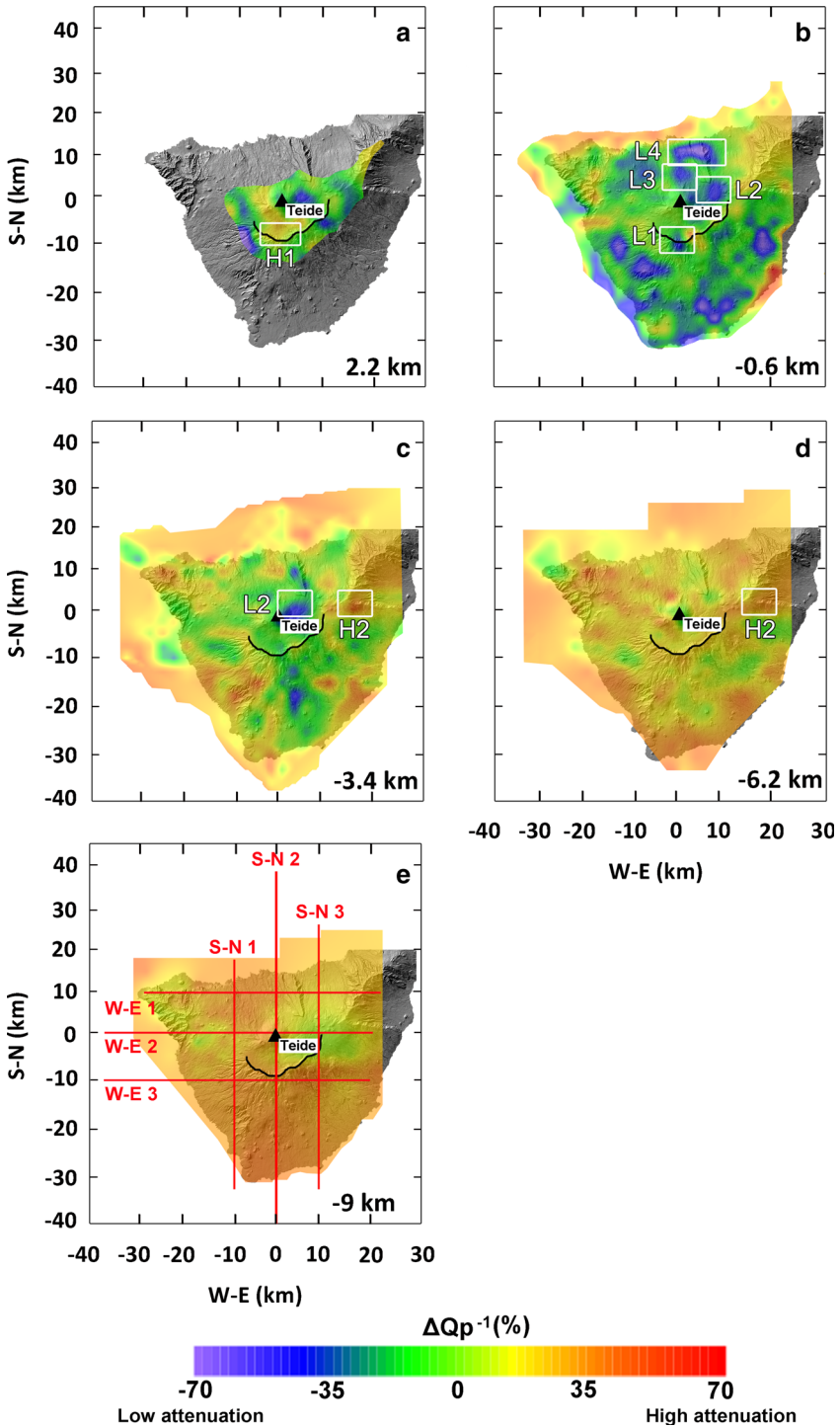
These rigid bodies additionally can act as reflecting or scattering structures. These structures can affect the composition of the coda waves of local seismograms, as observed by Del Pezzo et al. (1997) or can be identified as strong coherent arrivals in the coda of the used signal and draw the position of them as performed by De Barros et al. (2012). It is remarkable that anomalies L1, L2 and L3 were previously identified by the above authors using scattered seismic waves [(Fig. 8 from De Barros et al. (2012)]. These authors interpreted that these bodies as possible ancient magmatic chambers that fed eruptions of the last 2000 years occurred in Teide–Pico Viejo–Las Cañadas complex. In fact, these anomalous bodies could correspond to crystallized magma emplaced at the main rheological discontinuities that exist inside Tenerife, these being the base of the volcanic edifice (at 4–5 km b.s.l), the contact between Miocene sediments and the basaltic oceanic crust (5–7 km b.s.l) and the crust–mantle boundary (15–16 km b.s.l). The existence of magmatic reservoirs or underplating at such depths during certain stages in the evolution of Tenerife is also evidenced by the existing seismic reflection profiles (Watts et al. 1997; Dañobeitia and Canales 2000) and petrological data (Ablay 1997; Neumann et al. 1999; Thirlwall et al. 2000), which suggest that mafic magmas appearing on Tenerife have occasionally been evolving at such depths or equivalent pressures.

5. Outside of Las Cañadas caldera, we identify a low attenuation area marked in Figs. 7, 8 and 9 as L4 anomaly. This anomaly cannot be linked directly to the other structures. It is located in the north of Tenerife Island in a region called Orotava Valley (Fig. 1). This shallow low seismic attenuation zone can be interpreted as resulting from the high contrast exerted by the basaltic shield in a zone where the Cañadas edifice succession was removed by the formation of the landslide valley. This valley was subsequently infilled. This also suggests that the headwall of this valley does not affect the interior of the Cañadas caldera, thus supporting the idea that the caldera and the Icod valley resulted from two different destructive processes (see Martí et al. 1997).
6. There is an interesting high attenuation area located at intermediate depths (H2 in Figs. 7 and 8) which could be associated with recent eruptions. This zone is located below a region in which a strong fissural eruption took place at the beginning of the XVIII century (1704–05 Fasnía-Arafo-Siete Fuente eruptions, see Fig. 1) (Romero-Ruiz 1991). Making a vertical profile in Fig. 8d, on the top of H2 we identify a shallow high attenuation area that can be interpreted as the effect of volcanoclastic deposits of the eruptive processes. Between the surface and H2, the lower attenuation zone can be associated with cooled conduits, and H2 is the effect of the remaining hot materials at depth. This area is characterized also by low P-velocity. We can interpret the observed values as the effect of volcanoclastic deposits in surface combined with the remaining hot materials in depth.

## 5.2 Velocity Versus Attenuation

It is observed that P-wave velocity (García-Yeguas et al. 2012) and attenuation images match each other at shallow depths (from surface to 4–5 km depth). In this depth range, the





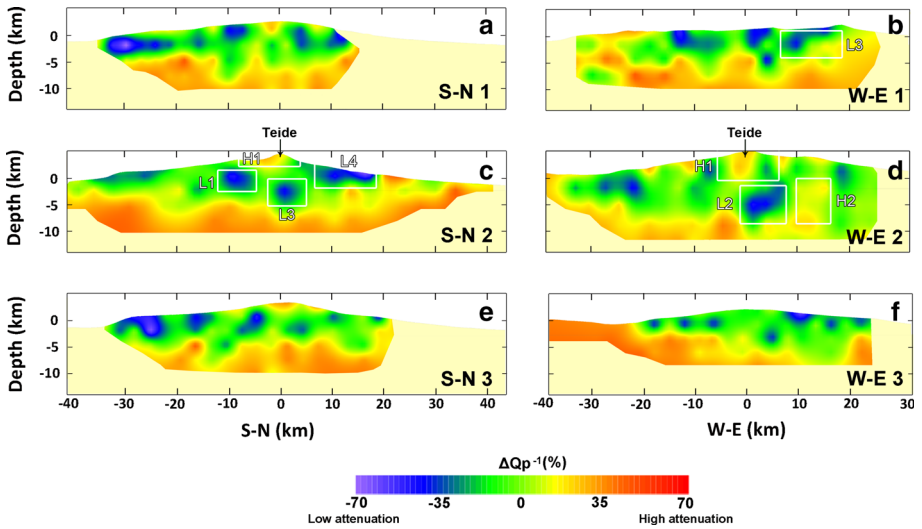


**Fig. 8** Results of the attenuation tomography model are shown in six vertical sections crossing the island (see Fig. 4): **a** SN 1, **b** WE 1, **c** SN 2, **d** WE 2, **e** SN 3 and **f** WE 3. The color scale show the variations (in percentage) of the attenuation model with respect to the average quality factor. The high and low attenuation anomalies discussed in the text are shown as red squares and red labels (H1, L1, L2, L3, L4)

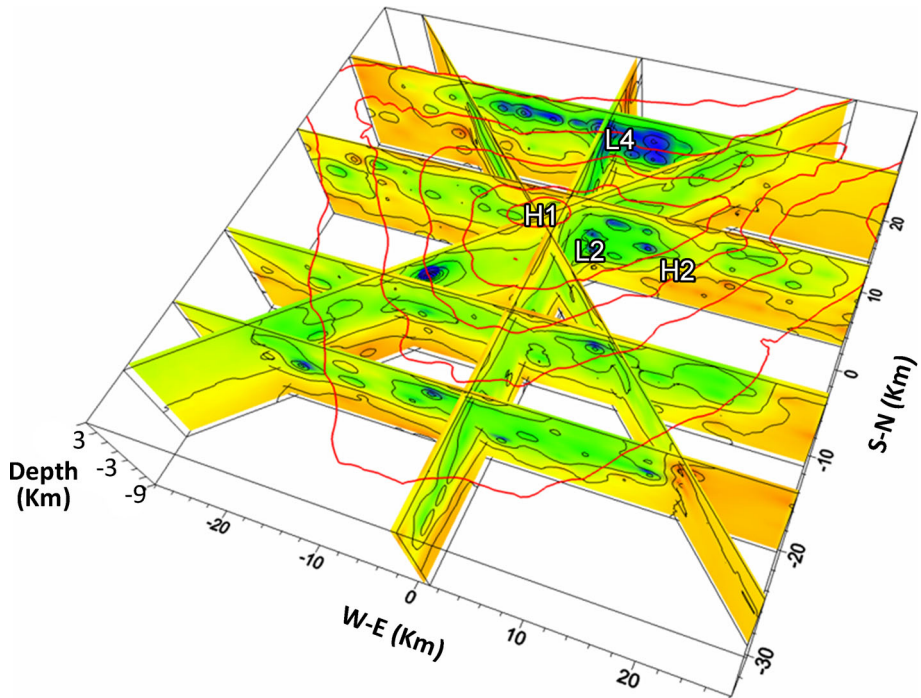


**Fig. 9** 3D perspective view of the final attenuation tomography model

coincidence between high-velocity and low attenuation zones predominates. The predominance of high attenuation corresponding to low velocity at surface is generally interpretable due to the presence of partially unconsolidated materials, with the possible presence of water layers. A completely different pattern can be observed at higher depths, where the high attenuation zone does not correspond to a low-velocity zone. This is possibly due to lack of resolution effects which could be present in the deepest borders of the volumes investigated with the velocity tomography, which unfortunately coincide with the zone with high attenuation. On the other hand, the high attenuation zone present at 6–10 km everywhere below Tenerife is well inside the optimal resolution achievable with the attenuation tomography technique utilized in the present paper.

### 5.3 Las Cañadas–Teide–Pico Viejo Complex Attenuation Structure

As indicated above, the cells size used for the inversion cannot permit us to solve with enough details some structures. However, the ray coverage shown in Fig. 2 suggests that the center of the island could be inverted with higher resolution. It is remarkable that this region is coincident with Las Cañadas–Teide–Pico Viejo complex. Around Teide volcano, there is a region of  $10 \times 10 \text{ km}^2$  in which cells of  $1.4 \times 1.4 \times 1.4 \text{ km}^3$  have optimal resolution (Fig. 10) up to a depth of 6 km b.s.l. Vertical attenuation profiles (N–S and W–E) are plotted in Fig. 10. The new images show that the maximum thickness of the collapsed zones, represented by the high attenuation H1 anomaly, of Las Cañadas caldera is between 1.5 and 2 km, coinciding with new structural estimates for the collapse of this caldera (Iribarren 2014). Other remarkable new results are the identification of two new small low attenuation bodies located just below the Teide–Pico Viejo volcanic complex (L5 and L6 in Fig. 10). They can be interpreted as old potential shallow magma reservoirs. The existence of these small ancient magma bodies has been frequently assumed to be located in this zone. When the Cañadas edifice was active, this zone accumulated most of the intrusions of deeper mafic magma in the central part the island due to the shadow effect that phonolitic chambers exerted on more deeper magma avoiding them to reach the surface at that zone (Martí and Gudmundsson 2000). In consequence, most of mafic magmas intruding below the shallow phonolitic systems crystallized there forming dense bodies of gabros, as is testified by high gravimetric positive anomalies (Ably and Kearey 2000; Gottsmann et al. 2008) and the present gabroid xenoliths in some Las Cañadas caldera forming pyroclastic deposits (Martí et al. 1994; Pittari et al. 2008). The same area seems to be the site today for the accumulation of deeper magmas that then differentiate and evolve into the phonolites that feed Teide–Pico Viejo eruptions, as is indicated by experimental petrology data (Andújar et al. 2010). Therefore, such small phonolitic reservoirs, assumed from the size of the last phonolitic eruptions (see Martí et al. 2008), have been able to be identified with the present higher resolution.

## 6 Conclusions

In the present work, we provide new observations and interpretations of the inner structure of the volcanic island of Tenerife based on the first high-quality 3D attenuation tomography. The seismic attenuation images are combined with previous geophysical, petrological and geological observations providing an integrated vision of the zone.

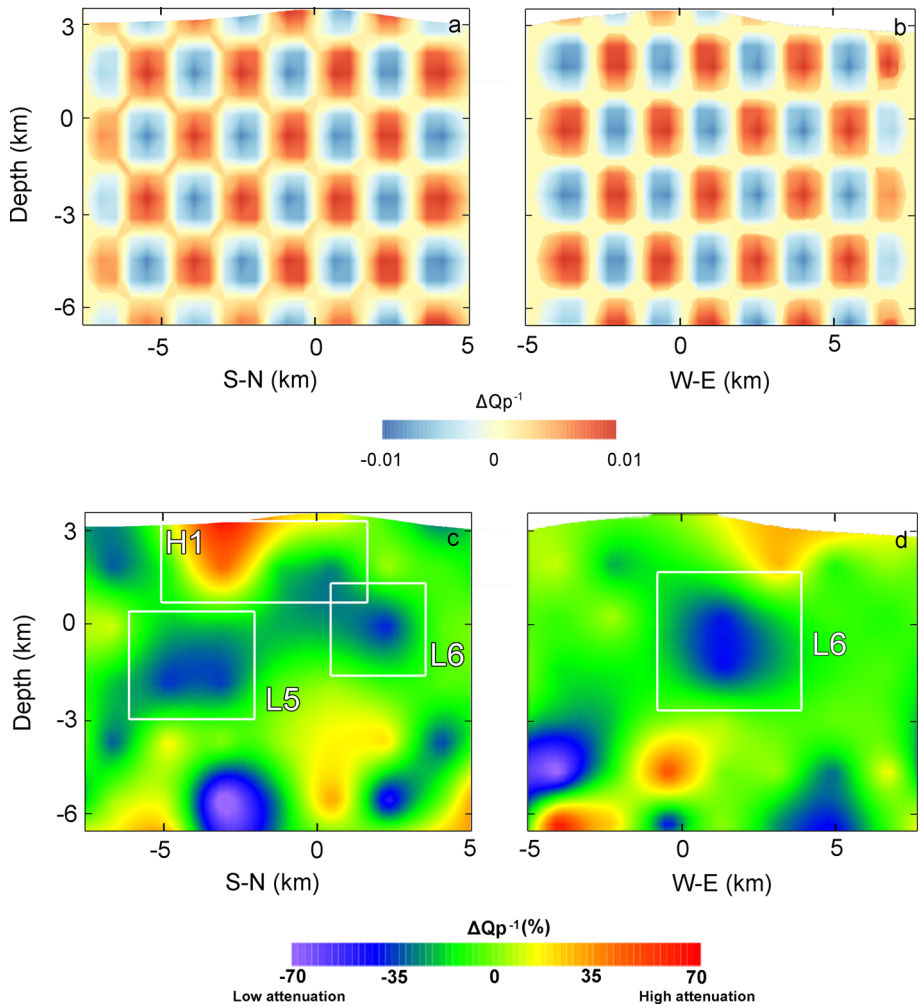


**Fig. 10** 3D perspective view of the final attenuation tomography model. High-resolution results of the attenuation tomography model are shown for Las Cañadas area (see Fig. 1) in two *vertical* sections (SN and WE). (0, 0) coordinates correspond to the position of Teide volcano, same as for SN 2 and WE 2 profiles in Fig. 8c, d but for a smaller area of  $10 \times 10 \text{ km}^2$ . *Top panels* (a, b) are the output of the checkerboard test. *Bottom panels* (c, d) are the obtained attenuation tomography results. New low attenuation areas L5 and L6 are marked

In general, the whole region is dominated by low attenuation structures, as expected for a volcanic environment. A first regional inversion with lower resolution allowed us to clearly associate the deeper high attenuation anomalies with the potential magma underplating predicted previously by several authors. The central zone of the island, characterized by a single low attenuation structure, is an additional evidence that could support the theory that Tenerife Island evolved in its origin from a potential single source rather than a possible three-arm structure. In this rigid structure, lowest attenuation anomalies are associated with intermediate-deep ancient magmatic chambers that could feed the volcanic

complex. At the surface, the island has strong attenuation contrasts. In some areas, high attenuation anomalies are evidenced, such as Las Cañadas edifice or the regions in which recent historical eruptions occurred. These high attenuation behaviors are interpreted as the combined effect of volcanoclastic deposits, sediments, multifracture structures, hydrothermal alterations or shallow aquifers. The shallow low attenuation body located in La Orotava valley could provide additional evidence that the destructive processes associated with this valley and Las Cañadas edifices could have originated independently.

Higher-resolution images performed around Teide volcano permitted us to better constrain the depth and size of the infilled Cañadas caldera and to identify a few cooled structures that could be associated with ancient shallow phonolitic reservoirs.

As a final conclusion, we can infer that the attenuation studies are a fundamental tool to better constrain the physical properties of volcanic regions and, therefore, contribute to solid arguments that could help to better understand the volcano dynamics.

**Acknowledgments** This work was funded by several projects as Grupo de Investigación en Geofísica y Sismología from the Andalusian Regional Program, APASVO (TEC2012-31551) Spanish project and by the EU project MED-SUV (EC-FP7 MEDiterranean SUPersite Volcanoes). MED-SUV has received funding from the European Union's Seventh Program for research, technological development and demonstration under grant agreement No 308665. We also want to acknowledge the very useful contribution of the Editor-in-Chief and an anonymous reviewer that helped us to improve the present paper. The first author is funded by the International Research Promotion Office from ERI (University of Tokyo), and Edoardo Del Pezzo was partially funded by the V2-Precursori project from DPC-INGV.

## References

- Abdel-Monen A, Watkins ND, Gast P (1972) Potassium-argon ages, volcanic stratigraphy and geomagnetic polarity history of the Canary Islands: Tenerife, La Palma and El Hierro. *Am J Sci* 272:805–825
- Ablay G (1997) Evolution of the Teide-Pico Viejo complex and magma system, Tenerife, Canary Islands. Ph.D. thesis, University of Bristol
- Ablay G, Kearey P (2000) Gravity constraints on the structure and volcanic evolution of Tenerife, Canary Islands. *J Geophys Res* 105:5783–5796
- Aki K (1980) Attenuation of shear-waves in the lithosphere for frequencies from 0.05 to 25 Hz. *Phys Earth Planet Inter* 21:50–60
- Akinci A, Del Pezzo E, Ibáñez J (1995a) Separation of scattering and intrinsic attenuation in southern Spain and western Anatolia (Turkey). *Geophys J Int* 121:337–353
- Akinci A, Ibáñez J, Del Pezzo E, Morales J (1995b) Geometrical spreading and attenuation of Lg waves: a comparison between western Anatolia (Turkey) and southern Spain. *Tectonophysics* 250:47–50
- Almendros J, Ibáñez J, Alguacil G, Morales J, Del Pezzo E, La Rocca M, Ortiz R, Araña V, Blanco MJ (2000) A double seismic antenna experiment at Teide volcano: existence of local seismicity and lack of evidences of volcanic tremor. *J Volcanol Geotherm Res* 103:439–462
- Almendros J, Ibáñez J, Carmona E, Zandomenighi D (2007) Array analyses of volcanic earthquake and tremor recorded at Las Cañadas caldera (Tenerife Island, Spain) during the 2004 seismic activation of Teide volcano. *J Volcanol Geotherm Res* 160:285–299
- Alparone S, Barberi G, Cocina O, Giampiccolo E, Musumeci C, Patané D (2012) Intrusive mechanism of the 2008–2009 Mt. Etna eruption: constraints by tomographic images and stress tensor analysis. *J Volcanol Geotherm Res* 229–230:50–63
- Ancochea E, Fúster JM, Ibarrola E, Cendrero A, Coello J, Hernan F, Cantagrel J, Jamond C (1990) Volcanic evolution of the Island of Tenerife (Canary Islands) in the light of new K-Ar data. *J Volcanol Geotherm Res* 44:231–249
- Andújar J, Costa F, Martí J (2010) Magma storage conditions of the last eruption of Teide volcano (Canary Islands, Spain). *Bull Volcanol* 72(4):381–395
- Araña V (1971) Litología y estructura del edificio Cañadas, Tenerife (Islas Canarias). *Estudios Geológicos* 27:95–137

- Blanco-Montenegro I, Nicolosi I, Pignatelli A, García A, Chiappini M (2011) New evidence about the structure and growth of ocean island volcanoes from aeromagnetic data: the case of Tenerife, Canary Islands. *J Geophys Res* 116:1–17. doi:[10.1029/2010JB007646](https://doi.org/10.1029/2010JB007646)
- Block LV (1991) Joint hypocenter-velocity inversion of local earthquakes arrival time data in two geothermal regions. Ph.D. dissertation, MIT, Cambridge
- Bosshard E, MacFarlane DJ (1970) Crustal structure of the western Canary Island from seismic refraction and gravity data. *J Geophys Res* 75(26):4901–4918
- Carracedo JC, Rodríguez-Bardiola E, Guillou H, Paterne M, Scaillet S, Pérez-Torrado FJ, Paris R, Fra-Paleo U, Hansen A (2007) Eruptive and structural history of Teide volcano and rift zone of Tenerife, Canary Islands. *Geol Soc Am Bull* 119:1027–1051
- Coppo N, Schnegg PA, Heise W, Falco P, Costa R (2008) Multiple caldera collapses inferred from the shallow electrical resistivity signature of the Las Cañadas caldera, Tenerife, Canary Islands. *J Volcanol Geotherm Res* 170:153–166
- Coppo N, Schnegg PA, Falco P, Costa R (2010) Conductive structures around Las Cañadas caldera, Tenerife (Canary Islands, Spain): a structural control. *Geol Acta* 8:67–82
- Dañoibeitia JJ, Canales JP (2000) Magmatic underplating in the Canary Archipelago. *J Volcanol Geotherm Res* 103(1):27–41
- Dash BP, Bosshard E (1969) Seismic and gravity investigations around the western Canary Islands. *Earth Planet Sci Lett* 7(2):169–177
- De Barros L, Martini F, Bean CJ, García-Yeguas A, Ibáñez J (2012) Imaging magma storage below Teide volcano (Tenerife) using scattered seismic wavefields. *Geophys J Int* 191:695–706
- De Gori P, Chiarabba C, Patané D (2005) Qp structure of Mount Etna: constraints for the physics of the plumbing system. *J Geophys Res* 110:1–16. doi:[10.1029/2003JB002875](https://doi.org/10.1029/2003JB002875)
- De Lorenzo S, Gasparini P, Mongelli F, Zollo A (2001) Thermal state of the Campi Flegrei caldera inferred from seismic attenuation tomography. *J Geodyn* 32:467–486
- De Siena L, Del Pezzo E, Bianco F, Tramelli A (2009) Multiple resolution seismic attenuation imaging at Mt. Vesuvius. *Phys Earth Planet Inter* 173:17–32
- De Siena L, Del Pezzo E, Bianco F (2010) Seismic attenuation imaging of Campi Flegrei: evidence of gas reservoirs, hydrothermal basins and feeding systems. *J Geophys Res* 115:2156–2174. doi:[10.1029/2009JB006938](https://doi.org/10.1029/2009JB006938)
- De Siena L, Waite G, Moran S, Thomas C (2013) Joint scattering and attenuation imaging of Mount Saint Helens reveals the melt paths feeding an erupting volcano. Submitted to *Nature Geosciences*
- De Siena L, Thomas C, Aster R (2014) Multi-scale reasonable attenuation tomography analysis (MuRAT): an imaging algorithm designed for volcanic regions. *J Volcanol Geotherm Res* 277:22–35
- Del Pezzo E (2008) Seismic wave scattering in volcanoes. *Adv Geophys* 50:353–371
- Del Pezzo E, La Rocca M, Ibáñez J (1997) Observations of high-frequency scattered waves using dense array at Teide volcano. *Bull Seismol Soc Am* 87:1637–1647
- Del Pezzo E, Bianco F, De Siena L, Zollo A (2006) Small scale shallow attenuation structure at Mt. Vesuvius. *Phys Earth Planet Inter* 157:257–268
- Domínguez Cerdeña I, Del Fresno C, Rivera L (2011) New insight on the increasing seismicity during Tenerife's 2004 volcanic reactivation. *J Volcanol Geotherm Res* 206:15–29
- Eberhart-Phillips D, Reyners M, Chadwick M, Chiu JM (2005) Crustal heterogeneity and subduction processes: 3-d vp, vp/vs and q in the southern North Island, New Zealand. *Geophys J Int* 162:270–288
- Fullea J, Camacho AG, Negro AM, Fernández J (2015) The Canary Islands hot spot: new insights from 3D coupled geophysical-petrological modelling of the lithosphere and uppermost mantle. *Earth Planet Sci Lett* 409:71–88. doi:[10.1016/j.epsl.2014.10.038](https://doi.org/10.1016/j.epsl.2014.10.038)
- Fúster JM, Araña V, Brande JL, Navarro JM, Alonso V, Aparicio A (1968) *Geología y volcanología de las Islas Canarias: Tenerife*. Instituto Mallada, CSIC, p 218
- García O, Guzmán S, Martí J (2014) Stratigraphic correlation of Holocene phonolitic explosive episodes of the Teide–Pico Viejo volcanic complex, Tenerife. *J Geol Soc* 171:375–387
- García-Yeguas A, Koulakov I, Ibáñez J, Rietbrock A (2012) High resolution P wave velocity structure beneath Tenerife Island (Canary Islands, Spain). *Geophys J Int* 117. doi:[10.1029/2011JB008970](https://doi.org/10.1029/2011JB008970)
- Geyer A, Martí J (2010) The distribution of basaltic volcanism on Tenerife, Canary Islands: implications on the origin and dynamics of the rift systems. *Tectonophysics* 483(3):310–326
- Gottsmann J, Camacho AG, Martí J, Wooler L, Fernández J, García A, Rymer H (2008) Shallow structure beneath the central volcanic complex of Tenerife from new gravity data: implications for its evolution and recent reactivation. *Phys Earth Planet Inter* 168:212–230
- Gudmundsson O, Finlayson DM, Itikarai I, Nishimura Y, Johnson W (2004) Seismic attenuation at Rabaul volcano, Papua new Guinea. *J Volcanol Geotherm Res* 130:77–92

- Hansen S, Thurber CH, Mandernach M, Haslinger F, Doran C (2004) Seismic velocity and attenuation structure of the east rift zone and south flank of Kilauea Volcano. *Hawaii Bull Seismol Soc Am* 94:1430–1440
- Ibáñez J, Del Pezzo E, Alguacil G, De Miguel F, Morales J, De Martino S, Sabbarese C, Posadas AM (1993) Geometrical spreading function for short-period *s* and coda waves recorded in southern Spain. *Phys Earth Planet Inter* 80:25–36
- Ibáñez J, Rietbrock A, García-Yeguas A (2008) Imaging an active volcano edifice at Tenerife Island, Spain. *EOS Trans Am Geophys Un* 89:289–300
- Iribarren I (2014) Modelos geológicos en 3D de la isla de Tenerife. Ph.D. thesis, University of Barcelona, p 234 (in Spanish)
- Koulakov I (2009) Code ATOM-3D for 3D tomographic inversion based on active refraction seismic data
- La Rocca M, Del Pezzo E, Simini M, Scarpa R, De Luca G (2001) Array analysis of seismogram from explosive sources: evidences for surface waves scattered at the main topographical features. *Bull Seismol Soc Am* 91:219–231
- Lodge A, Nippress S, Rietbrock A, García-Yeguas A, Ibáñez J (2012) Evidence for magmatic underplating and partial melt beneath the Canary Islands derived using teleseismic receiver functions. *Phys Earth Planet Inter* 212–213:44–54
- Mantovani E, Viti M, Babbucci D, Albarello D (2007) Nubia-Eurasia kinematics: an alternative interpretation from Mediterranean and North Atlantic evidence. *Ann Geophys* 50(3):341–366
- Martí J, Gudmundsson A (2000) The Las Cañadas caldera (Tenerife, Canary Islands): an overlapping collapse caldera generated by magma-chamber migration. *J Volcanol Geotherm Res* 103:161–173
- Martí J, Mitjavila J, Araña V (1994) Stratigraphy, structure and geochronology of the Las Cañadas caldera (Tenerife, Canary Islands). *Geol Mag* 131:715–727
- Martí J, Ablay G, Bryan S (1996) Comment on “The Canary Islands: an example of structural control on the growth of large oceanic-island volcanoes” by J. C. Carracedo. *J Volcanol Geotherm Res* 72(1):143–149
- Martí J, Hurlimann M, Ablay G, Gudmundsson A (1997) Vertical and lateral collapses on Tenerife (Canary Islands) and other volcanic ocean Islands. *Geology* 25:879–882
- Martí J, Geyer A, Andujar J, Teixó F, Costa F (2008) Assessing the potential for future explosive activity from Teide-Pico Viejo stratovolcanoes (Tenerife, Canary Islands). *J Volcanol Geotherm Res* 178:529–542
- Martí J, Sobradelo R, Felpeto A, García O (2012) Eruptive scenarios of phonolitic volcanism at Teide–Pico Viejo volcanic complex (Tenerife, Canary Islands). *Bull Volcanol* 74:767–782
- Martínez-Arevalo C, Patané D, Rietbrock A, Ibáñez J (2005) The intrusive process leading to the Mt. Etna 2001 flank eruption: constraints from 3D attenuation tomography. *Geophys ResLett* 32:L21,309
- Mezcua J, Buforn E, Udías A, Rueda J (1992) Seismotectonics of the Canary Islands. *Tectonophysics* 208:447–452
- Morozov IB (2011) Mechanisms of geometrical seismic attenuation. *Ann Geophys* 54(3):235–248. doi:[10.4401/ag-4780](https://doi.org/10.4401/ag-4780)
- Neumann ER, Wulff-Pedersen E, Simonsen S, Pearson NJ, O’Reilly SY, Martí J, Mitjavila J (1999) Evidence for fractional crystallization of periodically refilled magma chambers in Tenerife, Canary Islands. *J Petrol* 40:1089–1123
- Nolet G (2008) A breviary of seismic tomography. Imaging the interior of the earth and sun. Cambridge University Press, p 360, ISBN 978-0-521-88244-6
- Ohlendorf SJ, Thurber C, Pesicek JD, Prejean SG (2014) Seismicity and seismic structure at Okmok Volcano, Alaska. *J Volcanol Geotherm Res* 278:103–119
- Piña-Varas P, Ledo J, Queralt P, Marcuello A, Bellmunt F, Hidalgo R, Messeiller M (2014) 3-D magnetotelluric exploration of Tenerife geothermal system (Canary Islands, Spain). *Surv Geophys* 35:1045:1064
- Pittari A, Cas RAF, Wolff JA, Nichols HJ, Larson PB, Martí J (2008) The use of lithic clast distributions in pyroclastic deposits to understand pre-and syn-caldera collapse processes: a case study of the Abrego Ignimbrite, Tenerife, Canary Islands. *Dev Volcanol* 10:97–142
- Pous J, Schnegg PA, Muoz G, Martí J, Soriano C (2002) Magnetotelluric study of the Las Cañadas caldera (Tenerife, Canary Islands): structural and hydrogeological implications. *Earth Planet Sci Lett* 204:249–263
- Prudencio J, Del Pezzo E, García-Yeguas A, Ibáñez J (2013a) Spatial distribution of intrinsic and scattering seismic attenuation in active volcanic Islands, I: model and the case of Tenerife Island. *Geophys J Int* 195(3):1942–1956. doi:[10.1093/gji/ggt361](https://doi.org/10.1093/gji/ggt361)

- Prudencio J, Ibáñez J, García-Yeguas A, Del Pezzo E (2013b) Spatial distribution of intrinsic and scattering seismic attenuation in active volcanic Islands, II: deception Island images. *Geophys J Int* 195(3):1957–1969. doi:[10.1093/gji/ggt360](https://doi.org/10.1093/gji/ggt360)
- Prudencio J, De Siena L, Ibáñez J, Del Pezzo E, García-Yeguas A, Díaz-Moreno A (2015) The 3D attenuation structure of Deception Island Antarctica. *Surv Geophys* 36(3):371–390. doi:[10.1007/s10712-015-9322-6](https://doi.org/10.1007/s10712-015-9322-6)
- Roest WR, Dañoibeitia JJ, Verhoef J, Collette BJ (1992) Magnetic anomalies in the Canary Basin and the Mesozoic evolution of the central North Atlantic. *Mar Geophys Res* 14:1–24
- Romero-Ruiz C (1991) Las manifestaciones volcánicas históricas del archipiélago canario. Consejería Territorial Gobierno Autónomo de Canarias, Santa Cruz de Tenerife, España, p 1463
- Sato H, Fehler M, Maeda T (2012) Seismic wave propagation and scattering in heterogeneous earth, 2nd edn. Springer, Berlin, Heidelberg
- Schurr B, Asch G, Rietbrock A, Trumbull R, Haberland CH (2003) Complex patterns of fluid and melt transport in the central Andean subduction zone revealed by attenuation tomography. *Earth Planet Sci Lett* 215:105–119
- Soler-Javaloyes V, Carracedo JC (2013) Geophysical investigations of the Teide volcanic complex. Springer, Berlin, Heidelberg
- Thirlwall M, Singer BS, Marriner GF (2000)  $^{39}\text{Ar}/^{40}\text{Ar}$  ages and geochemistry of the shield stage of Tenerife, Canary Islands, Spain. *J Volcanol Geotherm Res* 103:247–297
- Tramelli A, Del Pezzo E, Fehler M (2009) 3D scattering image of Mt. Vesuvius. *Bull Seismol Soc Am* 99:1962–1972
- Um J, Thurber C (1987) A fast algorithm for two-point seismic ray tracing. *Bull Seismol Soc Am* 77:972–986
- Vanorio T, Virieux J, Capuano P, Russo G (2005) Three-dimensional tomography from P wave and S wave microearthquake travel times and rock physics characterization of the Campi Flegrei Caldera. *J Geophys Res* 110(B03201). doi:[10.129/2004JB003102](https://doi.org/10.129/2004JB003102)
- Verhoef J, Collette BJ, Dañoibeitia JJ, Roeser HA, Roest WR (1991) Magnetic anomalies off West-Africa (20–38 N). *Marin Geophys Res* 13(2):81–103
- Villasante-Marcos V, Finizola A, Abella R, Barde-Cabusson S, Blanco MJ, Brenes B, Cabrera V, Casas B, De Agustín P, Di Gangi F, Domínguez I, García O, Gomis A, Guzmán J, Iribarren I, Levieux G, López C, Luengo-Oroz N, Martín I, Moreno M, Meletlidis S, Morin J, Moure D, Pereda J, Ricci T, Romero E, Schutze C, Suski-Ricci B, Torres P, Trigo P (2014) Hydrothermal system of central Tenerife volcanic complex, Canary Islands (Spain), inferred from self-potential measurements. *J Volcanol Geotherm Res* 272:59–77
- Watts AB, Pierce C, Collier J, Dalwood R, Canales JP, Hens-Tock TJ (1997) A seismic study of lithosphere flexure in the vicinity of Tenerife, Canary Islands. *Earth Planet Sci Lett* 146:431–447
- Yoshimoto K, Sato H, Ohtake M (1993) Frequency-dependent attenuation of P and S waves in Kanto area, Japan, based on the coda-normalization method. *Geophys J Int* 114:165–174
- Zandomenghi D, Barclay A, Almendros J, Ibáñez J, Wilcock WSD (2009) Crustal structure of Deception Island volcano from P-wave seismic tomography: tectonic and volcanic implications. *J Geophys Res* 114:1–16. doi:[10.1029/2008JB006119](https://doi.org/10.1029/2008JB006119)